ACADEMIA ROMÂNĂ
Revue Roumaine de Chimie
http://web.icf.ro/rrch/

Rev. Roum. Chim.,
2014, *59*(11-12), 919-929

Dedicated to the memory of
Professor Candin Liteanu on his 100th anniversary

STRUCTURE AND PROPERTIES OF VANADIUM DOPED TiO_2 POWDERS PREPARED BY SOL-GEL METHOD

Irina STANCIU,[a,b] Luminita PREDOANA,[a,*] Crina ANASTASESCU,[a]
Daniela C. CULITA,[a] Silviu PREDA,[a] Jeanina PANDELE CUSU,[a] Cornel MUNTEANU,[a]
Adriana RUSU,[a] Ioan BALINT[a] and Maria ZAHARESCU[a]

[a] "Ilie Murgulescu" Institute of Physical Chemistry of the Roumanian Academy, 202 Spl. Independentei, 060021 Bucharest, Roumania
[b] Department of Mathematics and Fundamental Sciences, Maritime University, 104 Mircea cel Batran, 900663 Constanta, Roumania

Received September 30, 2014

The structure and properties of V doped TiO_2 nanometric powders, synthesized using sol-gel method were studied. The precursors employed were $Ti(OC_2H_5)_4$ as TiO_2 source and $VO(Acac)_2$ as V_2O_5 source. The molar ratios of TiO_2:V_2O_5 were 98:2 and 99.95:0.05, respectively. The obtained gels were thermally treated for 1 h at 300°C with a heating rate of 1°C/min in order to eliminate the water and organic residues and to obtain crystallized nanometric powders. The characterization of the powders was realized by thermogravimetric and differential thermal analysis (TGA/DTA), X-ray diffraction (XRD), scanning electron microscopy (SEM), infrared spectroscopy (FT-IR), specific surface area and porosity measurements. The obtained powders were also tested as catalyst for water splitting and oxidation of methanol. The correlation between composition, structure and catalytic properties of the samples was established.

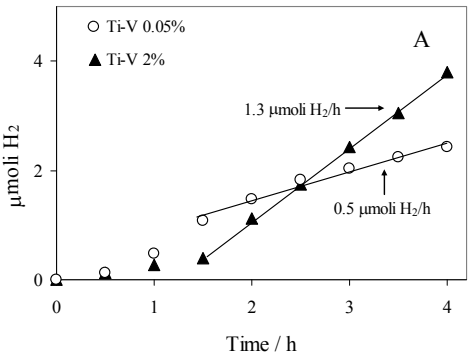

INTRODUCTION

TiO_2 has applications in various fields such as photocatalysis,[1,2] gas sensors, dye sensitized solar cells,[3-5] optical coatings, antimicrobial materials,[6] pigments, so on. As photocatalytic nanoparticles, titanium dioxide (TiO_2) is one of the most used materials due to its electrical and optical properties, low cost, chemical stability, and high photocatalytic activity. To enhance the photocatalytic performance of titanium dioxide, it has been doped with various metals, nonmetals and even co-doped.[7] Among metals, different transition metal ions: Pt^{4+}, Mo^{5+}, Mo^{+6}, V^{5+}, V^{4+}, Fe^{3+}, Ru^{3+}, Co^{3+}, Ag^{+}, Al^{3+},[8-12] rare earth elements: La^{3+}, Ce^{3+}, Er^{3+}, Pr^{3+}, Gd^{3+}, Nd^{3+}, Sm^{3+} [13, 14] or alkaline earth metals were used as dopants.[15, 16] Moreover, various researchers have co-doped titanium dioxide with metal-metal systems,[17-19] metal-nonmetal systems[20-22] or nonmetal-nonmetal systems.[23] The amount of dopant varies from 0.002 to 10 wt%.

Different methods are available for preparation of TiO_2 or doped TiO_2 materials. Among these methods, sol-gel technique is an efficient and

* Corresponding author: lpredoana@icf.ro or lpredoana@yahoo.com

versatile method for pure or doped TiO_2 films[24,25] or powder preparation.[26-28]

Based on the published data, it was concluded that the presence of dopants in titania lattice improves its photocatalytic activity. Most studies show that metal dopants should be used in small amounts, but the low content of metal doping leads to only small shift in the absorption edge of TiO_2 towards visible region. On the other hand, the use of high concentrations has adverse effects on photocatalytic properties of doped titania.[29]

Among metals, vanadium action has been extensively studied and most studies have reported that addition of vanadium ions can enhance the photoactivity of TiO_2 under illumination of visible light.[30-32] However, it has been also reported that the photocatalytic activity of TiO_2 doped with vanadium is less than of the bare TiO_2, under UV iradiation.

The amount of vanadium dopant varies from 0.001 mol%[33, 34] to 10 mol%.[35, 36]

In the present paper, the preparation by sol-gel method of V doped TiO_2 nanometric powders is discussed, as well as the influence of the amount of dopant on the structure and properties of the resulted nanopowders.

EXPERIMENTAL

Gels and powders preparation

The V-doped TiO_2 powders were prepared by the sol-gel method. The initial calculated compositions correspond to a TiO_2:V_2O_5 molar percentage of 98:2.0 and 99.95:0.05. $Ti(O\text{-}C_2H_5)_4$ (Merck) and $VO(acac)_2$ (Sigma-Aldrich) were used as starting precursors in ethanol medium. Acetylacetone (AcAc) (Sigma-Aldrich) was used as chelating agent. Nitric acid was used as catalyst. The obtained reaction mixture was homogenized at room temperature for 2 hours. The gelling occurred after 30 days in the case of the gel corresponding to 0.05% V_2O_5 and 40 days for the gel with 2.0% V_2O_5, showing a difference according to the V content. The obtained gels were dried at 100°C for 16 h, followed by a thermal treatment for 1 h at 300°C with a heating rate of 1°C/min. in order to eliminate the water and organic residues. The thermal treatment was established base on the TGA/DTA results.

In the synthesized samples the V content expressed as at%, represents 0.03at%V in the first composition and to 1.12at% when the composition was calculated for 2% V_2O_5.

The synthesized powders were labeled (Ti-V 0.05%) and (Ti-V 2.0%), respectively.

The composition of the initial solutions and the experimental conditions used are presented in Table 1.

Gels and powders characterization

The **thermal behavior** of the precursor gels were determined by differential thermal analysis and thermo-gravimetric analysis using a Mettler Toledo TGA/SDTA 851e equipment in Al_2O_3 crucibles and in flowing air atmosphere. The maximum temperature was set at 1000°C and the heating rate was of 5°C/min.

The **Fourier-transform infrared** (FT-IR) spectra of the gels and powders thermally treated were obtained using a Nicolet Spectrometer Nico 6700 FT-IR between 400 and 4000 cm^{-1}. The spectra were obtained using the KBr pellet technique. For each sample the spectra were recorded at a resolution of 4 cm^{-1} and processed using the OMNIC 7.3 software.

The **morphology** of the samples was investigated by scanning electron microscopy (SEM) using a high-resolution microscope, FEI Quanta 3D FEG model, operating at 20 kV, equipped with an energy dispersive X-ray (EDX) spectrometer Apollo X. The analyses were done in high vacuum mode, with Everhart–Thornley secondary electron detector.

The **X-ray measurements** were performed an Ultima IV X-Ray Diffractometer (Rigaku, Japan) using the Cu Kα radiation (Kα = 1.54056 Å) with a scan rate of 5°/min and 0.02° step size, at 40 kV and 30 mA. The diffraction pattern ranging between 10° and 80° was recorded.

Nitrogen sorption isotherms at -196°C were recorded on a Micromeritics ASAP 2020 automated gas sorption system. The samples were outgassed at 160°C for 3 h under vacuum prior to N_2 adsorption. Specific surface areas (S_{BET}) were calculated according to the Brunauer–Emmett–Teller (BET) equation using adsorption data in the relative pressure range between 0.05 and 0.30. The total pore volume (V_{total}) was estimated from the amount adsorbed at the relative pressure of 0.995. The pore size distribution curves were obtained using Barrett–Joyner–Halenda (BJH) method from the desorption branch.

Table 1

Composition of the initial solution and the experimental conditions of sol preparation

Sample	Reagents	Molar ratio				pH sol	Experimental conditions	
		TiO_2/V_2O_5	$\frac{ROH}{\sum precursor}$	$\frac{H_2O}{\sum precursor}$	$\frac{catalyst}{\sum precursor}$		T (°C)	t (h)
Ti-V 0.05%	$Ti(OC_2H_5)_4$ + $VO(Acac)_2$	98/2.0	36.5	1.35	0.35	3.5	25	2
Ti-V 2%	$Ti(OC_2H_5)_4$ + $VO(Acac)_2$	99.95/ 0.05	36.5	1.35	0.35	3.5	25	2

ROH = C_2H_5-OH

The photocatalytic tests were performed at 18°C in a quartz reactor loaded with 0.1 g of V-TiO_2 catalyst dispersed under stirring in a solution consisting of 110 mL ultrapure water (Millie-Q system >18MΩcm) and 10 mL CH_3OH. Methanol was used as sacrificial agent (hole scavenger to promote H_2 formation). The photoreactor was provided with a 5×5 cm^2 window made of optical quartz. The suspended catalyst was irradiated with 4.5×4.5 cm^2 light flux by a solar light simulating source (PEC–L 01, Japan) equipped with a 150 W short arc Xe lamp. The wave length of the standard solar spectrum AM 1.5 (1000 W/m^2) was between 350-1100 nm The photon flux entering in the reactor of the calibrated solar source was 1.7×10^{17} photons×cm^{-2}×s^{-1}.

During the photocatalytic tests, the reactor was bubbled with Ar carrier gas at a flow rate of 20 mL·min^{-1}. In order to prevent the lost of the liquid components, the reactor was topped with a condenser cooled at -5°C. The gaseous products of photocatalytic reaction (H_2 and CO_2) were analyzed by gas chromatography (Buck Scientific 910 equipped with TCD detectors) at 30 min time interval. The components of the gaseous mixture were separated and quantified using columns packed with 5 Å molecular sieve and Haysept. The photocatalytic activity was expressed as μmol of H_2 and CO_2 produced in one hour normalized to 1g of photocatalyst.

RESULTS AND DISCUSSION

As prepared gels

Following the gelling process in the experimental conditions presented above, transparent amorphous gels were obtained according to the XRD results (not presented here).

FTIR spectroscopy

The FT-IR spectra of V doped titanium dioxide gels are shown in Fig. 1.

The vibration bands around 3400 cm^{-1} and 1630 cm^{-1} are present in both samples and correspond to hydroxyl groups linked with titanium atoms (Ti-OH) and to surface-adsorbed water.[37]

In the same time some vibration bands assigned to the reagents used in the synthesis could be noticed (1382 cm^{-1} assigned to NO_3^- from the nitric acid used as catalyst and at 1287 cm^{-1} assigned to δCH_3 from AcAc).

The low intensity band at 2420 cm^{-1} can be attributed to physical CO_2 gas absorbed at the surface of material.[38] The band around 574 cm^{-1} could be assigned to νTi-O of condensed octahedral (TiO_6) with a small displacement. In our case this band is shifted to higher values of wavelength due to interaction between TiO_2 and V.

Thermal analysis

In order to establish the thermal process required for elimination of the adsorbed water and organic residues from the synthesized gels, thermogravimetric and differential thermal analysis (TGA/DTA) were used.

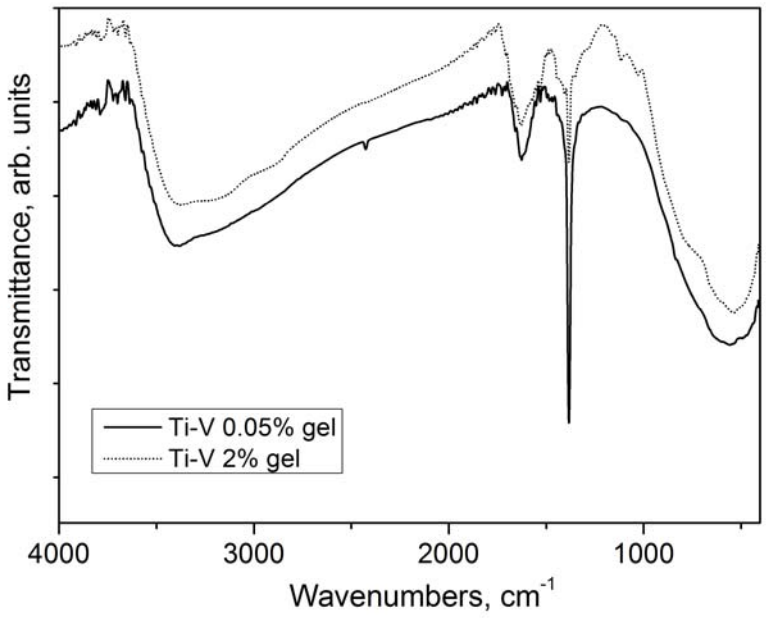

Fig. 1 – IR spectra of the synthesized V-doped TiO_2 gels.

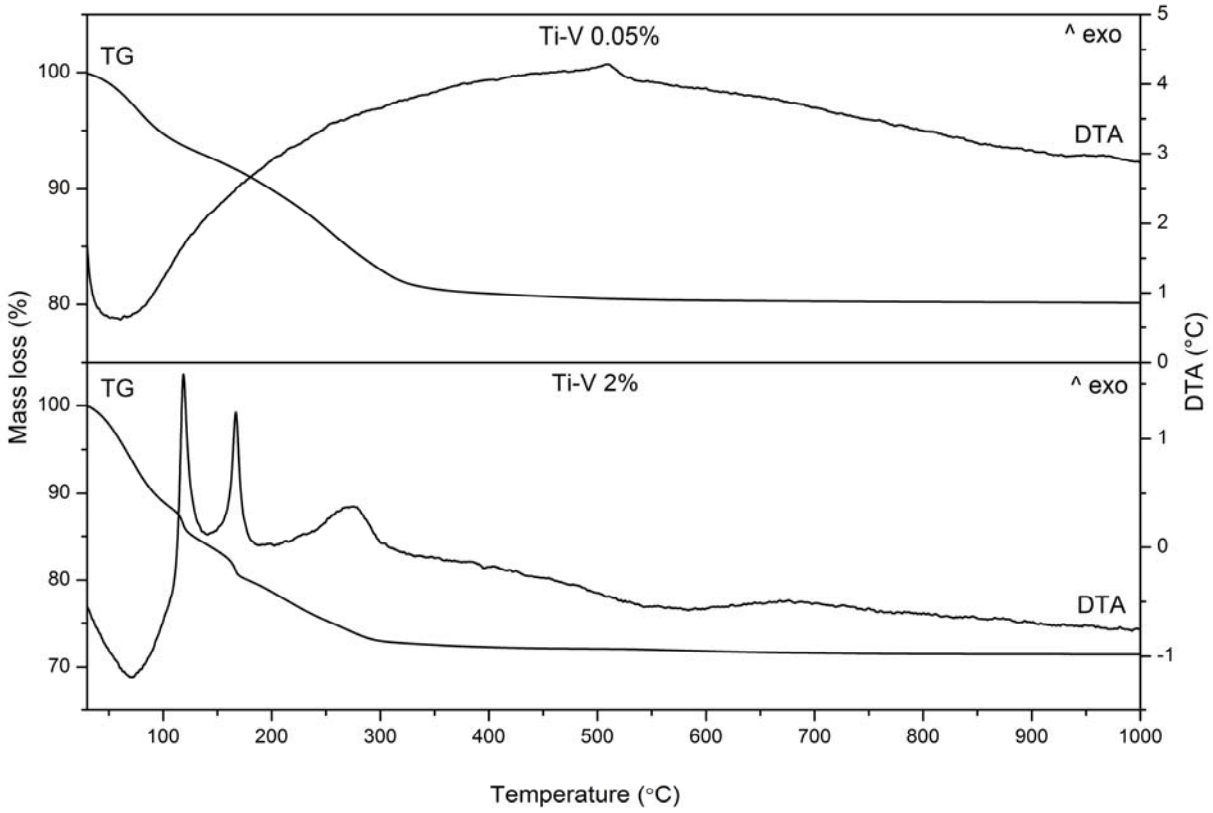

Fig. 2 – DTA/TGA curves of the synthesized samples.

In Fig. 2 the TGA/DTA curves for the sample Ti-V 0.05% and the similar curves for the sample Ti-V 2% corresponding to the decomposition of obtained gels are shown, while in the Table 2 the thermal effects and their assignment are presented.

It could be noticed that the decomposition occurs step-wise with a noticeable weight loss in the case of sample with Ti-V 2% (21%) and with a smaller weight loss in case of sample Ti-V 0.05% (10.5%), in the 100-200°C temperature range.

The differences in the behavior of the two samples could be correlated to their composition and the reagents used in synthesis. In both cases, as V reagent, $VO(acac)_2$ was used that reacts with the $Ti(O\text{-}C_2H_5)_4$ during the sol-gel process producing acetylacetonate derivates that remains embedded in the obtained gels. By thermal treatment they are eliminated in the mentioned temperature range. For example, the acetylacetone boiling temperature is 140°C. In the sample Ti-V 2% the weight loss is higher than in the case of sample Ti-V 0.05% and it is accompanied by two corresponding exothermal effects.

In the 200-500°C temperature range, for both samples a weight loss of around 8% is assigned to the decomposition and elimination of organic species and structural hydroxyl groups.

At higher temperatures not significant weight loss is observed and the exothermal effect noticed could be correlated to the powders crystallization.

Based on the DTA/TGA results, the samples were thermally treated at 300°C for 1 h.

Powders resulted by thermal treatment of the gels

In accordance with the TGA/DTA results, the samples obtained were thermally treated at 300°C for 60 min, using a heating rate of 1°C/min.

SEM-EDX results

The morphology of the obtained powders was determined by SEM investigations. The SEM images presented in Fig. 3, show the presence of very small particles (<10 nm) with a very low degree of crystallization but with a very high tendency to agglomerate. No differences were noticed depending on the amount of V in the powders composition.

The EDX analysis revealed the presence of V only in the case of Ti-V 2% sample (1.1% at.), in the amount closely to the predicted value (Fig. 4).

Table 2

TGA/DTA results for Ti-V samples

Sample	Temperature range, (°C)	Thermal effects, (°C)		Weight loss, (%)	Assignement
		Endo	Exo		
Ti-V 0.05%V	20-200	85		10.5	Physically absorbed water and solvent elimination; decomposition and elimination of organic species
	200-500			8.8	Decomposition and elimination of organic species and hydroxyl groups elimination
	500-1000		510	0.5	Crystallization
				∑=19.8	
Ti-V 2%V	20-200	72	115 165	21	Physically absorbed water and solvent groups elimination; decomposition and elimination of organic species
	200-500		273	7	Decomposition and elimination of organic species and hydroxyl groups elimination
	500-1000			0.5	-
				∑=28.5	

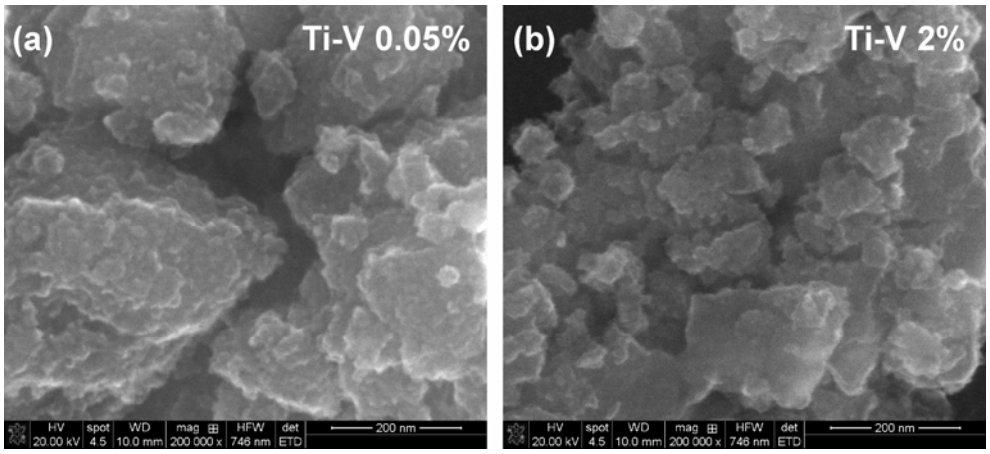

a) b)

Fig. 3 – SEM images of, a) sample Ti-V 0.05%V and b) sample Ti-V 2%V.

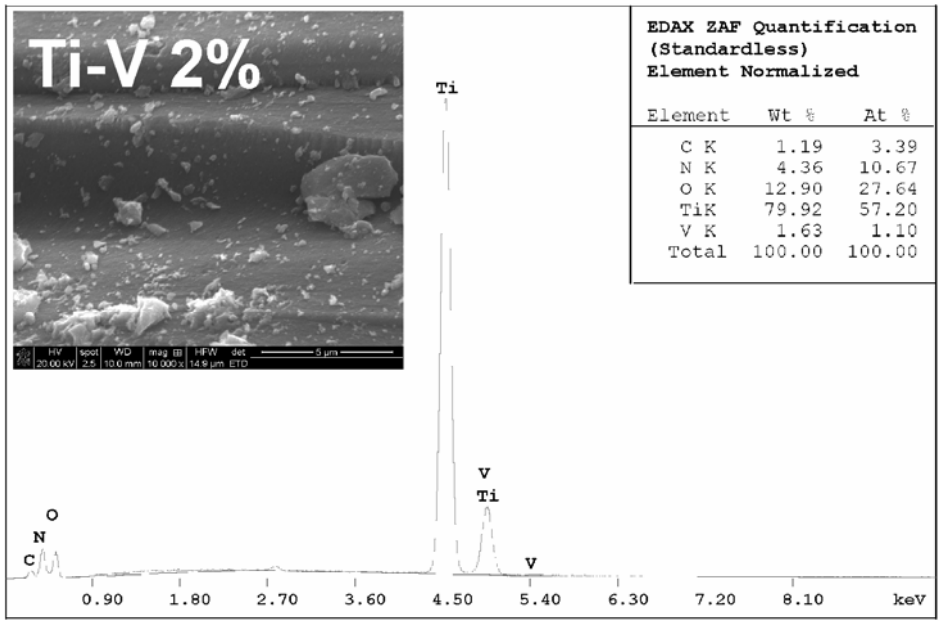

Fig. 4 – EDX spectra of Ti-V 2%.

X-Ray diffraction

In Fig. 4 the XRD patterns of the samples are presented. The lattice constants of anatase phase were calculated using the Whole Pattern Powder Fitting module of Rigaku's PDXL software and are listed in Table 3.

The X-ray patterns of the two samples indicate the presence of two phases. The main phase was identified as anatase, according with ICDD file no. 00-021-1272 and the secondary phase is a solid solution with rutile structure formed between the two oxides, according to ICDD file no. 00-032-1378.

FTIR spectroscopy

The FT-IR spectra of the gels thermally treated at 300°C for 1 hour, are presented in Fig. 5 and the comparative assignment of the vibration bands to those noticed in the initial gels are summarized in Table 3.

From the data presented in Table 3 one may observe that by thermal treatment some vibration bands assigned to the reagents used in the synthesis vanished (1382 cm^{-1} assigned to the presence of NO_3^-, 1287 cm^{-1} assigned to the presences of AcAc) and the vibration bands in the 3000-3500 cm^{-1} domain, corresponding to the hydroxyl groups linked with titanium atoms (Ti-OH), diminished. In the same time, the vibration band assigned to the Ti-O-Ti network increases, showing a network ordering.

In literature is highlighted the importance of the hydroxyl groups linked with titanium atoms (Ti-OH) for catalytic reactions, because they turn into hydroxyl radicals which are strong oxidizing under UV conditions.[39,40]

V doped TiO_2 shows strong peak at 500-550 cm^{-1} which can be attributed to Ti–O bond in the TiO_2 lattice.[41]

BET specific surface area and porosity

The nitrogen adsorption – desorption isotherms of the V-doped TiO_2 are shown in Fig. 6. Both isotherms are type IV according to the IUPAC classification[42] and the hysteresis loops are of type H_2. This type of hysteresis can be observed in the pores with narrow neck and wider bodies (ink-bottle pores). For the sample Ti-V 2%, the hysteresis loop is very narrow and appear in the range of relative pressure between 0.35 – 0.55. The insert in Fig. 6 magnifies the isotherm of Ti–V 2% sample in the range where the hysteresis appears. In case of Ti-V 0.05% sample the hysteresis loop is a bit larger and appears at relative pressure between 0.35 – 0.7. The desorption branch is steeper than that of the adsorption branch in the same range of relative pressures. This feature is characteristic of mass-transfer-limited filling and emptying of non-uniform or partially blocked uniform pores.[43] This change of the hysteresis loops shape can be explained as a result of the increasing mesopore size. The pore size distribution for both samples is monomodal and relatively narrow (Fig. 7).

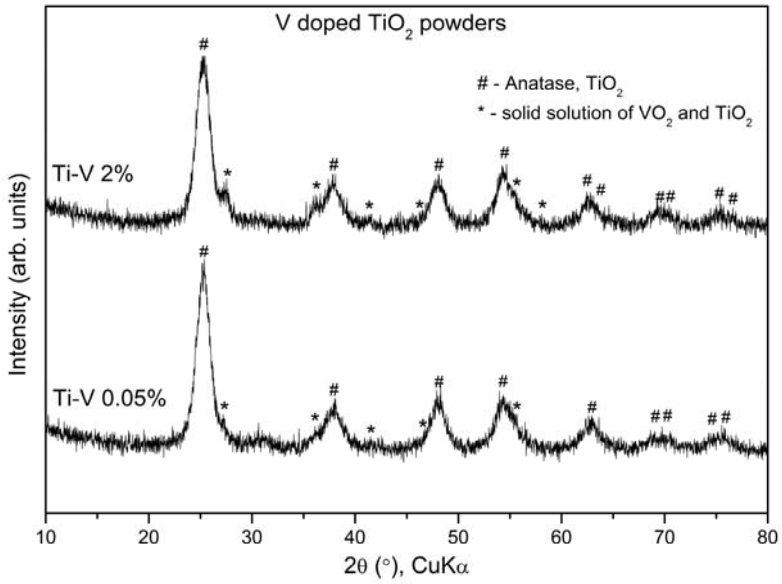

Fig. 4 – The XRD patterns of the samples thermally treated at 300 °C.

Table 3

Lattice constants of anatase phase in the syntesized samples

Sample	a=b (Å)	c (Å)	α=β=γ (°)
Ti-V 0.05%	3.783(5)	9.462(11)	90
Ti-V 2%	3.7861(19)	9.479(6)	90

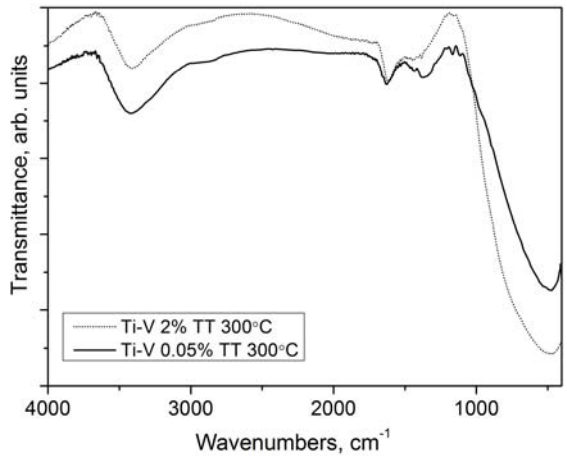

Fig. 5 – FT-IR spectra of the obtained powders by thermal treatment of the gels.

Table 3

The assignment of the vibration bands in IR spectra of the samples

Wavenumber/cm^{-1}				Assignments and vibration mode
Ti-V 0.05% gel	Ti-V 2%gel	Ti-V 0.05% TT	Ti-V 2% TT	
3405	3414	3420	3411	νOH structural OH group
2923		2923	2923	
2850		2847	2847	
2423	2420			CO_2 absorption
1628	1634	1631	1615	δH_2O adsorbed water
1382	1382			νNO_3^-
	1287			δCH_3 from AcAc
	691			Ti-O-Ti
558	574			νTi-O
		485	482	Ti-O-Ti

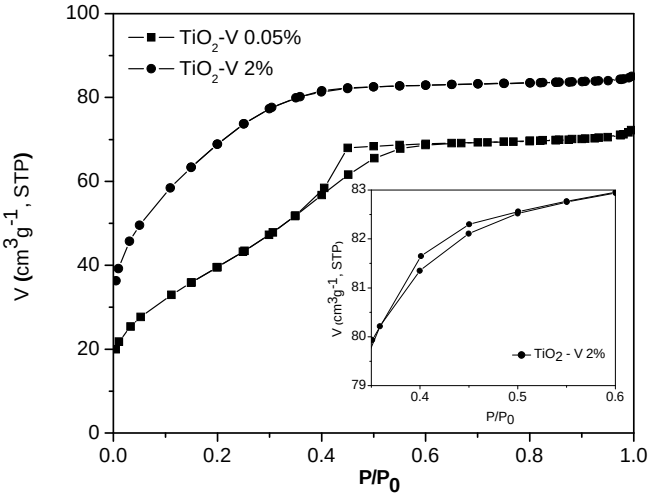

Fig. 6 – N_2 adsorption–desorption isotherms of Ti-V 0.05% and Ti-V 2%
(insert magnifies the isotherm of Ti-V 2% sample in the range of hysteresis loop).

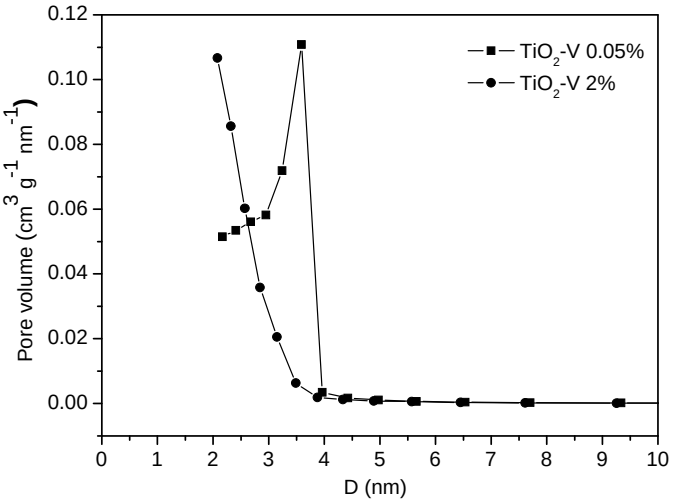

Fig. 7 – Pore size distribution of Ti-V 0.05% and Ti-V 2%.

Table 4

BET surface area (S_{BET}), total pore volume (V_{total}) and pore size (D) of the samples

Sample	S_{BET} (m^2/g)	V_{total} (cm^3/g)	D (nm)
Ti-V 0.05%	150.1	0.11	3.1
Ti-V 2%	242.7	0.13	2.5

The textural parameters (specific surface area (S_{BET}), total pore volume (V_{total}) and average pore diameter (D)) are summarized in Table 4. As can be seen, as the percent of V was increased, the S_{BET} and V_{total} increased from 150.1 to 242.7 m^2/g and from 0.11 to 0.13 cm^3/g, while the average pore diameter decreased from 3.1 to 2.5 nm.

Comparing the structure and thermal behavior of the synthesized samples it was noticed that they have a similar structure (majority anatase and very low-content of V-doped rutile) and their thermal decomposition takes place in the same temperature range.

Higher differences were established for their BET specific surface area and porosity. It is assumed that a difference of about 100 m^2/g in the value of the specific surface area will influence their photocatalytic activity.

Photocatalytic tests

The photocatalytic tests under simulated solar light were carried out in order to observe whether improvements are achieved when TiO_2 host material is doped with V_2O_5. Previous studies reported that the vanadium doping has a beneficial effect on the photocatalytic activity of TiO_2.[39] The decrease of TiO_2 band gap by V doping is considered to be the main reason for the observed activity enhancement. The reported red shift observed in band gap absorption seems to confirm this hypothesis.[44] The Ti-V catalysts were tested for photodegradation of natural and synthetic dyes under visible light[45,46] as well as for the photomineralization of organic pollutants.[47]

The comparative results of the photocatalytic tests for Ti-V 0.05% and Ti-V 2% catalysts obtained for solar light irradiation are presented in Fig. 8 (A, B). The figures show the time course of the cumulative amounts of gaseous products (H_2, CO_2) generated photocatalytically. The reaction rates, expressed as μmol H_2 or CO_2/g of catalyst was calculated in the linear domain of the activity plots, after the steady state was established. Typically, lower reaction rates can be observed in the first 1.5 h of reaction time. The steady state (linear dependence of reactant amount on time) was reached after the solution was saturated with H_2 and CO_2 at 18°C.

Fig. 8 presents comparatively the time course of H_2 (A) and CO_2 (B) formation over the Ti-V 0.05% and Ti-V 2% respectively. The TiO_2 with higher V content (2%) was more active to produce H_2 (1.3 μmol H_2/h) compared to the sample with low vanadium content (Ti-V 0.05%, 0.5 μmol H_2/h). The total amount of H_2 formed in 4 h under sun light irradiation was 3.5 and 2.5 μmol H_2 for Ti-V 2% and Ti-V 0.05%, respectively.

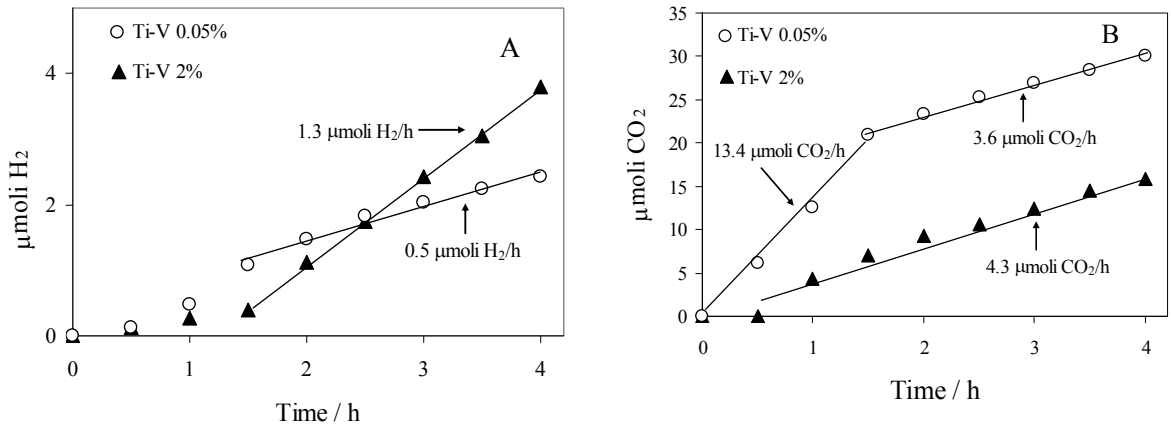

Fig. 8 – Comparative H_2 (A) and CO_2 (B) evolvement over Ti-V 0.05% (○) and Ti-V 2% (▲).

The rate of CO_2 formation in the linear domain was relatively close for the two investigated catalysts; respectively 3.6 μmol CO_2/h over Ti-V 0.05% and 4.3 μmol CO_2/h over Ti-V 2%, respectively (see Fig. 8B). Fig. 8B shows that the catalyst with lower V content was more active to produce CO_2 in the first 1.5 h (≈13.4 μmol CO_2/h). However, for longer reacting time, the rate of CO_2 formation decreased, reaching the steady state value of 3.6 μmol CO_2/h. Except the induction period of 0.5 h, the rate of CO_2 formation over Ti-V 0.05% was constant (4.3 μmol CO_2/h, see Fig. 8B).

One important information concerning the mechanism of photochemical reaction over the two investigated catalytic materials can be obtained from the analysis of the CO_2/H_2 molar ratio. In steady state conditions (linear dependence of the amount of formed gaseous products on time), the CO_2/H_2 ratios were 7.2 and 3.3 for Ti-V 0.05% and Ti-V 2%, respectively. It should be mentioned that the concentration of residual oxygen in reactor was ≈ 0.5%. This information should be taken into consideration when interpreting the experimental data, because the oxidation of methanol occurs in parallel with the water splitting. This fact explains the formation in excess of CO_2 compared to H_2. For a pure water splitting process, using methanol as sacrificial reagent, the ratio H_2/CO_2 should be three. The following equations, describing the overall process (water splitting and methanol oxidation), can be derived from the experimentally obtained data:

$$7.2\ CH_3OH + 10.3\ O_2 \xrightarrow{0.05\%\ V/TiO_2} 7.2\ CO_2 + H_2 + 13.4\ H_2O \quad (1)$$

$$3.3\ CH_3OH + 4.45\ O_2 \xrightarrow{2\%\ V/TiO_2} 3.3\ CO_2 + H_2 + 5.6\ H_2O \quad (2)$$

The reactants and products stoichiometry depicted in above equations suggest that Ti-V 0.05% catalyst behaves mostly as a photooxidation catalyst. In contrast, the higher H_2/CO_2 ratio for Ti-V 2% catalyst means an increased contribution of the photochemical water splitting to the overall process. However, in this case too, the oxidation of methanol prevails over the water splitting process. One suitable and suggestive as well term describing the overall photochemical process can be photo reforming of methanol.[48]

Based on the experimental results, the following main steps can be proposed: (i) the photo generation of e^- (electron) in conduction band and h^+ (holes) in the valence band of the catalyst, (ii) the electron transfer to surface-adsorbed O_2 with the formation of the superoxide radical $O_2^{\bullet-}$ which is transformed in aqueous media in reactive $HO^\bullet$ radical, (iii) methanol oxidation by h^+ and or $HO^\bullet$ with the formation of CO_2.[49] The V dopant enhances probably the oxidizing ability of TiO_2 by accelerating the electron and hole transfer to O_2 [step (ii)] and methanol [step (iii)] catalyzing thus the complete oxidation of organic substrate to CO_2. The role of methanol sacrificial reagent is to react rapidly with the photogenerated holes and hydroxy radicals in order to decrease the rate of electron-hole recombination.[48]

Future research plans should include the investigation of the relationship between specific lattice defects formation in TiO_2 by V doping and photocatalytic activity for methanol reforming.

CONCLUSIONS

V-doped TiO_2 nanopowders powders with different V content were synthesized by sol-gel method in alcoholic medium.

The powders were characterized from the point of view of their structure, morphology, thermal behaviour and adsorption properties. The catalytic properties of the samples were also investigated.

It has been established that the different amount of V for TiO_2 doping (0.05% or 2.0% V_2O_5) did not influence in major extent the structural and thermal properties of the samples, but have influenced their morphological and catalytic properties.

The sample doped with the higher amount of V has shown a higher surface area as compared with the sample with lower V content.

The comparative results of the photocatalytic tests of the Ti-V 2% and Ti-V 2% samples obtained for solar light irradiation have shown that the Ti-V 0.05% catalyst show better results for water splitting while Ti-V 0.05% catalyst is more active in methanol oxidation.

Further investigations are underway in order to elucidate in more details the catalytic properties of the samples for solar light irradiation.

Acknowledgments: This paper was carried out within the research programme "Materials Science and Advanced Methods for Characterization" of "Ilie Murgulescu" Institute of Physical Chemistry, financed by the Roumanian Academy. Support of the EU (ERDF) and Roumanian Government, which allowed for acquisition of the research infrastructure under POS-CCE O 2.2.1 project INFRANANOCHEM - Nr. 19/01.03.2009, is gratefully acknowledged. Project – **PN-II-PT-PCCA-2013-4(0864)-(94/2014)** – "Cleanphotocoat" is acknowledged.

REFERENCES

1. V. Belessi and D. Petridis, "Modified and Nonmodified TiO_2 Nanoparticles for Environmental Applications", Chapter 13, in "The Role of Colloidal Systems in Environmental Protection", Elsevier, 2014, p. 289-330.
2. M. Tahir and N.A.S. Amin, *Energ. Convers. Manage.*, **2013**, *76*, 194-214.
3. B. O'Regan and M. Grätzel, *Nature*, **1991**, *353*, 737-740.
4. E. Enache-Pommer, J.E. Boercker and E.S. Aydil, *Appl. Phys. Lett.*, **2007**, *91*, 123116.
5. A. Dumbrava, A. Georgescu, G. Damache, C. Badea, I. Enache, C. Oprea and M.A. Girtu, *J. Optoelectron. Adv. M.*, **2008**, *10*, 2996-3002.
6. X. Wei, Z. Yang, S.L. Tay and W. Gao, *Appl. Surf. Sci.*, **2014**, *290*, 274-279.
7. U.G. Akpan and B.H. Hameed, *Appl. Catal. A-Gen.*, **2010**, *375*, 1-11.
8. S.N.R. Inturi, T. Boningari, M. Suidan and P.G. Smirniotis, *Appl. Catal. B-Environ.*, **2014**, *144*, 333-342.
9. M.A. Rauf, M.A. Meetani and S. Hisaindee, *Desalination*, **2011**, *276*, 13-27.
10. S. Liu, T. Xie, Z. Chen and J. Wu, *Appl. Surf. Sci.*, **2009**, *255*, 8587-8592.
11. J. Zheng, H. Yu, X. Li and S. Zhang, *Appl. Surf. Sci.*, **2008**, *254*, 1630-1635.
12. S.-M. Chang and W.-S. Liu, *Appl. Catal. B-Environ.*, **2014**, *156-157*, 466-475.
13. A.-W. Xu, Y. Gao and H.-Q. Liu, *J. Catal.*, **2002**, *207*, 151-157.
14. Y. Wang, H. Cheng, L. Zhang, Y. Hao, J. Ma, B. Xu and W. Li, *J. Mol. Catal. A-Chem,* **2000**, *151*, 205-216.
15. Y. Li, S. Peng, F. Jiang, G. Lu and S. Li, *J. Serb. Chem. Soc.*, **2007**, *72*, 393-402.
16. N. Venkatachalam, M. Palanichamy, B. Arabindoo and V. Murugesan, *Catal. Commun.*, **2007**, *8*, 1088-1093.
17. J. Reszczynska, T. Grzyb, J.W. Sobczak, W. Lisowski, M. Gazda, B. Ohtani and A. Zaleska, *Appl. Surf. Sci.*, **2014**, *307*, 333-345.
18. M. Khan, J. Li, W. Cao and A. Ullah, *Sep. Purif. Technol.*, **2014**, *130*, 15-18.
19. X. Yang, F. Ma, K. Li, Y. Guo, J. Hu, W. Li, M. Huo and Y. Guo, *J. Hazard. Mater.*, **2010**, *175*, 429-438.
20. X. Yang, C. Cao, K. Hohn, L. Erickson, R. Maghirang, D. Hamal and K. Klabunde, *J. Catal.*, **2007**, *252*, 296-302.
21. Y. Gu, M. Xing and J. Zhang, *Appl. Surf. Sci.*, **2014**, *319*, 8-15.
22. H. Sun, G. Zhou, S. Liu, H.M. Ang, M. O Tadé and S. Wang, *Chem. Eng. J.*, **2013**, *231*, 18-25.
23. L. Pan, J.-J. Zou, S. Wang, Z.-F. Huang, X. Zhang and L. Wang, *Appl. Surf. Sci.*, **2013**, *268*, 252-258.
24. M. Crisan, M. Zaharescu, D. Crisan, R. Ion and M. Manolache, *J. Sol-Gel Sci. Techn.*, **1998**, *13*, 775-778.
25. Z. Liu, J. Ya, L. E, Y. Xin and W. Zhao, *Mater. Chem. Phys.*, **2010**, *120*, 277-281.
26. T. Dascalescu, L. Todan, A. Rusu, S. Preda, C. Andronescu, D. Culita, C. Munteanu and M. Zaharescu, *Rev. Roum. Chim.*, **2014**, *59*, 125-134.
27. H. Khan and D. Berk, *Reac. Kinet. Mech. Cat.*, **2014**, *111*, 393-414.
28. J. Choi, H. Park and M.R. Hoffmann, *J. Mater. Res.*, **2010**, *25*, 149-158.
29. R. Jaiswal, N. Patel, D.C. Kothari and A. Miotello, *Appl. Catal. B-Environ.*, **2012,** *126*, 47– 54.
30. M. Bettinelli, V. Dallacasa, D. Falcomer, P. Fornasiero, V. Gombac, T. Montini, L. Romano and A. Speghin, *J. Hazard. Mater.*, **2007**, *146*, 529-534.
31. J.C.-S. Wu and C.-H. Chen, *J. Photoch. Photobio. A*, **2004**, *163*, 509-515.
32. H. Li, G. Zhao, Z. Chen, G. Han and B. Song, *J. Colloid Interf. Sci.*, **2010**, *344*, 247-250.
33. Y.-H. Lin, W.-C. Hung, Y.-C. Chen and H. Chu, *Aerosol Air Qual. Res.*, **2014**, *14*, 280-292.
34. R.-a. Doong, P.-Y. Chang and C.-H. Huang, *J. Non-Cryst. Solids*, **2009**, *355*, 2302-2308.
35. K. Bhattacharyya, A.K. Patra, P.U. Sastry and A.K. Tyagi, *J. Alloy. Compd.*, **2009**, *482*, 256-260.

36. T.-B. Nguyen, M.-J. Hwang and K.-S. Ryu, *Appl. Surf. Sci*., **2012**, *258*, 7299-730.
37. J. Liu, R. Yang and S. Li, *Rare Metals*, **2006**, *25*, 636-642.
38. L. Todan, T. Dascalescu, S. Preda, C. Andronescu, C. Munteanu, D.C. Culita, A. Rusu, R. State and M. Zaharescu, *Ceram. Int.*, **2014**, *40*, 15693-15701.
39. H. Khan and D. Berk, *J. Sol-Gel Sci. Techn*., **2013**, *68*, 180-192.
40. K.J. Deng, K.L. Lv, H.S. Zuo, J. Sun, S.C. Liu, X.F. Li and D.Y. Wang, *J. Hazard. Mater*., **2009**, *161*, 396-401.
41. I. Othman, R.M. Mohamed and F.M. Ibrahem, *J. Photoch. Photobio. A*, **2007**, *189*, 80-85.
42. K.S.W. Sing, D.H. Everett, R.A.W. Haul, L. Moscou, R.A. Pierotti, J. Rouquerol and T. Siemieniewska, *Pure Appl. Chem*., **1985**, *57*, 603-619.
43. M.S. Hamdy, *J. Mol. Catal. A-Chem*., **2014**, *393*, 39-46.
44. J.C.-S.Wu and C.-H. Chen, *J. Photoch. Photobio. A*, **2004**, *163*, 509-515.
45. M. Mokhtarimehr, A. Eshaghi and M. Pakshir, *New J. Ceram. Glass*, **2013**, *3*, 87-90.
46. J. Choi, H. Park and M.R. Hoffmann, *J. Mater. Res*., **2010**, *25*, 149-158.
47. S. Klosek and D. Raftery, *J. Phys. Chem. B*, **2001**, *105*, 2815-2819.
48. A. Patsoura, D.I. Kondarides and X.E. Verykios, *Catal. Today*, **2007**, *124*, 94-102.
49. O. Carp, C.L. Huisman and A. Reller, *Prog. Solid State Ch*., **2004**, *32*, 33-177.